International Journal of Mechanics and Energy (IJME)
Vol. 11, Issue 2, 2024, ISSN: 2286-5845

Strong coupling fluid–structure interactions of a turbine impeller in a stirred vessel

Sarhan Karray*, Zied Driss, Hedi Kchaou, Mohamed Salah Abid
Laboratory of Electro-Mechanic Systems (LASEM), National School of Engineers of Sfax (ENIS), University of Sfax (US), B.P. 1173, Road Soukra km 3.5, 3038 Sfax, TUNISIA

Abstract: In this paper, a coupling algorithm is developed in a partitioned approach using strong scheme to provide the time history of the fluid flow and structure parameters. These parameters affect the unsteady behaviour of the turbine since the blades are flexible. Exploring the repressed area of the turbine, this allows to follow the passing of the baffle front of the turbine blades and the deformation of the blade, in particular. The fluid flow is governed by the Navier–Stokes equations for incompressible viscous fluids and modelled with the finite volume method. The structure is represented by a finite element formulation. The control of the history time of the fluid flow and structure parameters, such as the three components of velocity, turbulent kinetic energy, its dissipation rate and the blade displacement enables to understand the mass transfer phenomenon. This will show the effect of the interaction between the various components of the geometry system. Predictions of the numerical results have been compared to the literature data, and a satisfactory agreement has been found.
Key words: Computational Fluid Dynamics (CFD), Computational structure Dynamics (CSD), fluid-structure interaction (FSI), Strong coupling algorithm, Turbine.

1. Introduction

The coupling of unsteady fluid flow and structure motion has been of paramount importance to the field of computational mechanics ([1]; [2]; [3]). The elastic structure deforms due to the fluid action, mainly pressure and viscous stress. The rapid development of computing software, such as Computer-Aided Engineering (CAE) and Computer Fluid Dynamics (CFD), offers unified standard data form, which is accepted by both fluid mechanics and solid mechanics. In such case, people can run the CFD and CSD code simultaneously and exchange numerical data on the interfaces in order to understand the coupling effect [4]. The between a fluid flow and a deforming structure is referred to as fluid–structure interaction (FSI). The latter has been of major interest in many fields, such as collapses of bridges [5], the stability and responses of aircraft wings [6] and turbine blades [7]. The complicated non-uniform and unsteady turbulent flow often induces intensive oscillation of the flexible structure. Inversely, the vibration of the flexible structure has a strong influence on the time-space distribution of the flow. In the biomedical field, the interaction between an elastic artery ([8]; [9]) or a heart chamber [10] and the blood that flows through them is of a big interest. Also, for the design of artificial heart valves ([11]; [12]), the fluid–structure interaction needs to be taken into account.

Two numerical methods are distinguished as either monolithic, or, partitioned. In the monolithic approach, the system of fluid flow and solid displacement equations are solved simultaneously and are discretized in time and space in the same manner ([13]; [14]; [15]; [16]; [17]). This direct approach is known to be highly robust and stable for very strong fluid–structure interaction including, for example, phase transformation in material processing, viscoplastic deformation, fracturing due to shock or detonation

*** Corresponding author:** Sarhan Karray
E-mail: sarhan.karray@isgis.usf.tn.

([18]; [19]). However, monolithic methods represent a less modularity and require more coding than the partitioned approach in which the flow and structural equations are solved using independent suitable algorithms and discretization methods ([20]; [21]). Partitioned schemes have gained popularity thanks to their modularity, possible re-use of separate efficient solvers and their scalability potential ([22]; [23]; [24]). For example, each solver may employ a very efficient – possibly physics-based – precondition. Similarly, a need may arise for a new material type or formulation (e.g. from compressible to nearly incompressible) to be implemented. Partitioned methods can be further classified into weak [6] and strong coupling [25]. The weak coupling schemes are also called staggered methods because the equations governing the dynamics of the fluid and the structure are solved in an alternating manner. In the strong coupling scheme, the fluid and the structure are treated as elements of a single dynamical system, and all of the governing equations are integrated simultaneously and interactively in the time domain.

Some theoretical and numerical studies of strong partitioned coupling for one and two dimensional problems are found in [26]. Commercial codes for combining existing solvers have been developed. Glück [27] applied a partitioned coupling between the CFD code (FASTEST-3D) and the CSD code (ASE) to thin shells and membranous structures with large displacements. The latter method has been modified and coupled by MpCCI. Bucchignani [28] presented a numerical code to study the problem of an incompressible flow in a stirred vessel. It is based on a method of a partition treatment type, with the fluid and structural fields resolved by coupling two distinct models. [4] provided an effective new idea to solve the aeroelastic problem using Fluent and ABAQUS/ANSYS. Baek [25] have developed, analyzed and validated a new approach for stabilizing fluid–structure interactions suitable for partitioned algorithms. We have employed a high-order method and hence it is more susceptible to instabilities arising from the coupling of the two different domains i.e. fluid (code NEKTAR) and structure (code Stress NEKTAR). These two solvers, NEKTAR and Stress NEKTAR, are coupled through sub-iterations, with overall spectral accuracy in space and 2nd-order accuracy in time. Habchi [21] have developed a partitioned solver, taking into account strong coupling fluid–structure interaction problems. The use of such approach is fundamental in the case of partitioned methods where different solvers for the fluid flow and the structural deformation are communicating at the fluid–structure interface.

This paper presents a strong coupling of partitioned fluid–solid interaction solvers in a stirred vessel equipped with a turbine impeller. The hydrodynamic behaviour of the turbine impeller was studied numerically ([29]; [30]; [31]). In their work the latter authors have studied the turbine impeller in laminar regime. Other works are concerned with the thermal performance of the agitation mobile while determining the overall exchange coefficient ([32]; [33]). However, they did not take into account the effect of the structure. These observations led to the numerical hydromechanics study. Here, we study the turbulent flow in a stirred vessel as well as the mechanical deformation of the structure. For this purpose, a strong coupling algorithm was used to provide a detailed account for the temporal evolution of the characteristics of the fluid. These characteristics have a strong influence on the unsteady behaviour of the blades since it is flexible. This allows us to explore the delivery zone of the turbine impeller, to follow the process of the baffle before passing the blades of the turbine and the deformation of the blade. The control of the history time of the various flow parameters such as the three components of velocity, the turbulent kinetic energy, its dissipation rate and the mechanical deformation allows a better understanding of the mass transfer phenomenon. This helps see the effect of the interaction between the various constituent parts of the geometry system. The content of this paper is organized as

follows: Section 2 describes the geometry of the system. Section 3 provides the governing equations of the fluid and the structure. Section 4 describes the computational simulation for both parts. Section 5 presents the numerical results. Finally, section 6 contains concluding remarks.

2. Geometry system

The system was made by a flat bottom, cylindrical vessel of diameter D = 300 mm, and the liquid height in the vessel was H = D. A turbine of e = 1 mm thickness was attached to the inside wall of the cylindrical tank. It has four blades of d = 0.5 D diameter (Fig. 1). The clearance between the bottom of the mixing vessel and the blade tip was z = 0.5 D. The turbine rotated in a clockwise direction when viewed from above. The origin of the coordinate system is located in the bottom of the vessel (Fig. 1). The geometry of the system resembled the one that has already been experimented by [34]. In the following investigations, the fluid used in the CFD simulation is the water defined by the density and the viscosity that are equal to $\rho = 1000$ Kg/m^3, $\mu = 1$ MPs, respectively. The flow is fully turbulent where the Reynolds number and the Froude number are equal to $Re = 10^4$ and Fr= 0.02, respectively. The structure is assumed to be isotropic linear and elastic material law is applied. Its mechanical characteristics are defined by a Young modulus equals to E = 210 MPa, a Poisson's ratio equal to ν=0.28 and a yield stress equals to σ = 215 MPa.

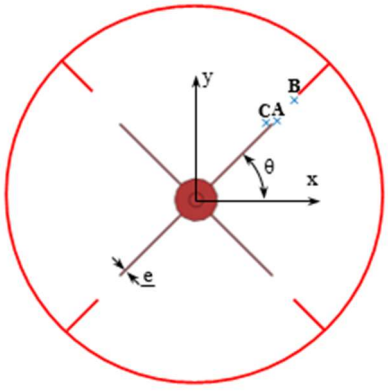

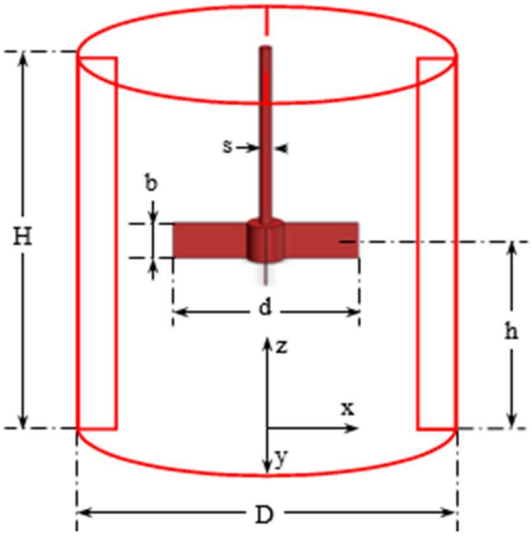

Fig. 1. Stirred vessel equipped with a turbine

3. Governing equations

It was already pointed out, in section 1, that an FSI problem is actually a two-field problem. Therefore, its mathematical description involves the governing equations of the fluid and the structural parts, which will be given in sections 3.1 and 3.2, respectively. The fluid-structure interaction is modelled via special boundary conditions at the interface for each sub problem, which will be presented in section 3.3. In the following investigations, the fluid is assumed to be incompressible and Newtonian. The structure is assumed to be isotropic linear, and elastic material law is applied.

3.1 The Fluid field

The problem is governed by the continuity equation and the incompressible Navier-Stokes equations; both in three-dimensional forms:

$$\mathrm{div}\ \vec{V} = 0 \tag{1}$$

$$\frac{\partial(\rho\vec{V})}{\partial t} + \mathrm{div}\left(\rho\,\overrightarrow{\vec{V}} \otimes \vec{V} + p\,\bar{\bar{I}}\right) = \mathrm{div}(\bar{\bar{\tau}}) \tag{2}$$

The momentum equation is a statement of conservation of momentum in each of the three component directions. The three momentum equations are written in a rotating frame of reference. Therefore, the centrifugal and the Coriolis acceleration terms are added to the momentum equations. The k-ε model used by Launder et al. (1974) is often used in process engineering, and particularly, in the simulation of mixing problems. The standard k-ε turbulence equations are given in the following forms:

$$\frac{\partial k}{\partial t} + \mathbf{div}\left[\vec{V}\ k - \frac{2}{\pi}\left(\frac{d}{D}\right)^2 \frac{1}{Re}\left(1 + \frac{\upsilon_t}{\sigma_k}\right)\overrightarrow{grad k}\right] = \frac{2}{\pi}\left(\frac{d}{D}\right)^2 \frac{1}{Re} G - \varepsilon \quad (3)$$

$$\frac{\partial \varepsilon}{\partial t} + \mathbf{div}\left[\vec{V}\varepsilon - \frac{2}{\pi}\left(\frac{d}{D}\right)^2 \frac{1}{Re}\left(1 + \frac{\upsilon_t}{\sigma_\varepsilon}\right)\overrightarrow{grad \varepsilon}\right] = \frac{\varepsilon}{k}\left[C_{c1}\frac{2}{\pi}\left(\frac{d}{D}\right)^2 \frac{1}{Re} G - C_{c2}\varepsilon\right] \quad (4)$$

The turbulent kinetic energy production takes the following form:

$$G = \upsilon_t\left[2\left[\left(\frac{\partial U}{\partial r}\right)^2 + \left(\frac{\partial V}{r\,\partial\theta} + \frac{U}{r}\right)^2 + \left(\frac{\partial W}{\partial z}\right)^2\right] + \left[\frac{\partial V}{\partial r} - \frac{V}{r} + \frac{\partial U}{r\,\partial\theta}\right]^2 + \left[\frac{\partial W}{r\,\partial\theta} + \frac{\partial V}{\partial z}\right]^2 + \left[\frac{\partial U}{\partial z} + \frac{\partial W}{\partial r}\right]^2\right] \quad (5)$$

The k-ε model is based on the concept of turbulent viscosity where k and ε are calculated by solving the above equations (3) and (4). The value of the kinematic turbulent viscosity is deduced from the following equations:

$$\upsilon_t = C_\mu \frac{\pi}{2}\left(\frac{D}{d}\right)^2 Re\ \frac{k^2}{\varepsilon} \quad (6)$$

3.2 The Structure field

In this work, elastic isotropic structures were used considered. The continuity equation and the balance of the momentum equation are given in the following forms:

$$\frac{D\rho_s}{Dt} + \mathrm{div}\left(\rho_s \overrightarrow{V_s}\right) = 0 \quad (7)$$

$$\rho_s \frac{D\overrightarrow{V_s}}{Dt} - \overrightarrow{\mathrm{div}}\,\overline{\overline{\sigma}} = \vec{f} \quad (8)$$

The hypoelastic law is presented in the following form:

$$\overline{\overline{\sigma}} = 2\mu_s \overline{\overline{\varepsilon}} + \lambda \mathrm{tr}(\overline{\overline{\varepsilon}})I \quad (9)$$

The strain tensor is defined as follows:

$$\overline{\overline{\varepsilon}} = \frac{1}{2}\left(\overrightarrow{\mathrm{grad}\vec{u}} + \left(\overrightarrow{\mathrm{grad}\vec{u}}\right)^T\right) \quad (10)$$

With:

$$\overrightarrow{V_s} = \frac{\partial \vec{u}}{\partial t} = \ddot{\vec{u}} \quad (11)$$

3.3 Fluid-structure interface

The fluid-structure interface represents the contact mechanics problem between an elastic structure and the fluid flow. This requires the characterization of boundary conditions exchanged and describe the interaction between the fluid and the structure. We use two conditions on the level of the interface. These conditions are given in the following forms:

$$\vec{V}\vec{n} = \overrightarrow{V_s}\vec{n} \quad (12)$$

$$\overline{\overline{\sigma}}\vec{n} = \overline{\overline{\tau}}\vec{n} \quad (13)$$

With:

$$\vec{n} = \vec{n}_f = -\vec{n}_s \quad (14)$$

4. Computational simulation

In order to make a computational simulation for the fluid-structure interaction phenomenon, we used a coupling algorithm to deal with problems of strongly non-linear FSI. This algorithm is based on a partitioned method. This method determines the structure and fluid solution vector, independently from each other, updating afterwards the relevant boundary conditions (Fig. 2). This algorithm requires a CSD code, a CFD code and a coupling interface.

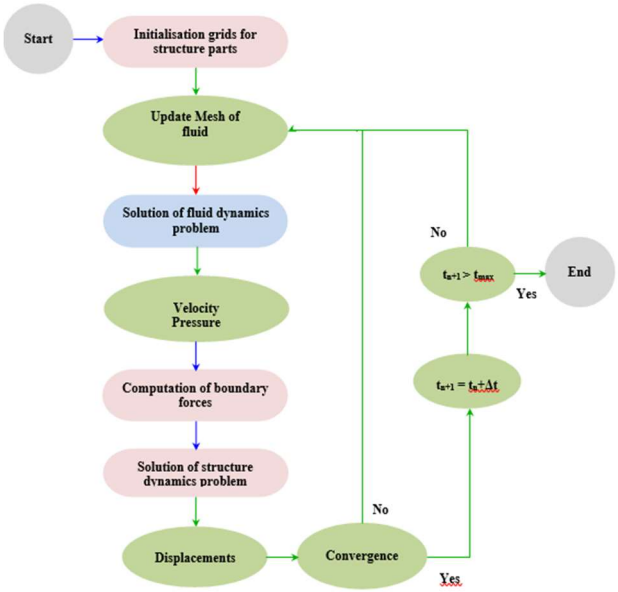

Fig. 2. Coupling algorithm

4.1 The CSD code

The CSD code allows the static calculation of the structure and solves the partial differential equations (Eq. (7) and (8)) of the model chosen for the structure. More precisely, this code must be able to receive information representing the varying physical forces in time exerted by the fluid on the fluid-structure interface. On the other hand, this code is used to determine the displacement of the nodes.

4.2 The CFD code

The CFD code allows the hydrodynamic calculation of the fluid, and solves the equations of Navier-stokes (Eq. (1) and (2)) for the model chosen for the fluid. The finite volume method is adopted for the treatment of these equations. Initially, the fluid field is being divided into elementary volumes representing the geometry of the problem. Secondly, the differential equations are discretised using the control volume approach [35]. The appropriate equations in the range of the turbulent incompressible Newtonian fluid flow are expressed in the general conservation. Several quantities can be found. These are the velocity field, the pressure, the turbulent kinetic energy and its dissipation rate. In a fluid problem, we need to know the pressure value at the level of the fluid structure interface. In addition, this code must be able to receive information representing displacement of the structure part to be used to solve the fluid flow problem.

4.3 The CFD code

The coupling between the fluid and the structure occurs at the interface between the two domains. The coupling conditions comprise a data-transfer operation between the fluid and the structure. Specifically, we are interested in the transfer values of the forces exerted on the structure. When this structure deforms, it, then, focuses on the transfer of the fluid displacement values. These conditions must check the continuity of the velocity and continuity of efforts. Our coupling interface is programmed in FORTRAN. It allows (Fig. 3):

- Receive calculated by the CFD code as a file "Force.dat 'strengths and convert it into an executable file" Fichier.inp "CSD code.

- Receive displacements calculated by the CSD code as a file "Fichier.rep" and convert it into an executable file "Nxyz.dat" in CFD code.

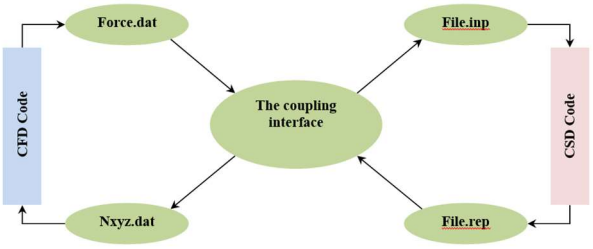

Fig. 3. Data transfer between the two codes

5. Results and discussions

Following the application of the strong coupling algorithm, we present the temporal evolution of parameters, such as, the three components of velocity, pressure, displacement and the turbulent kinetic energy

and its dissipation rate. For this reason, we have chosen three points A, B and C located at the end of the blade, respectively, at the baffle and downstream of the blade (Fig. 1). In this work, the flow is fully turbulent where the Reynolds number and the Froude number are equal to Re = 10^4 and Fr= 0.02, respectively.

5.1 At the end of the blade (point A)

5.1.1 Radial velocity component

Fig. 4 shows the time history of the radial velocity component for a point (A) located at the end of the blade, as shown in Fig. 1. Globally, a periodic fluctuation of this velocity component is observed for 0.2 second, which corresponds to 100 time steps. This fluctuation is due to the interaction between the turbine blades and baffles. For a rotational frequency of 265.4 rad / min, four baffles perform 4.44 rad / s, then these amounts to saying that each baffle made 3.52 passages (point A) in 0.2 second. For each component of the velocity, we note that the period of fluctuation is constant. She left about 30 times step is 30 m.s. In addition, the low frequency variations have been observed in each period varying between a minimum and another maximum because of the weak interaction between the impeller and the baffles.

During the passage of the front baffle blade (point A), the radial velocity reaches a minimum value. Therefore, we can infer that the jet created by the turbine is no longer a radial jet. Fig. 4(a) shows the evolution of the radial velocity over time with the use of a CFD code. Nevertheless, Fig. 4(b) shows the evolution of the radial velocity over time following application of an algorithm, which examines the coupling interaction between the impeller and the baffles. In Fig. 4, the problem of interaction does not affect the radial velocity component for the great similarity between the two curves of temporal changes.

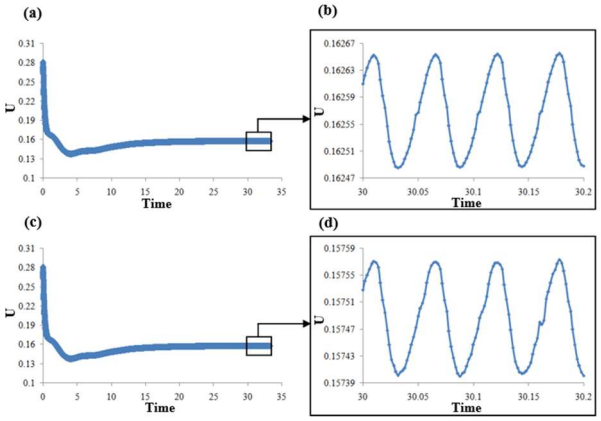

Fig. 4. Time history of the radial velocity component U

5.1.2 Tangential velocity component

Fig. 5(a) shows the tangential velocity component as a function of time with the use of a CFD code. Besides, fig. 5(b) shows the time history of the tangential velocity following application of an algorithm that examines the coupling interaction between the impeller and the baffles. Based on these results, we see the periodic fluctuations of the tangential component of the velocity due to the weak interaction between the moving agitator and the baffles. However, we noted that the tangential component is at a maximum level during the passage of the chicane before the blade (point A). This shows that the rotation of a turbine with four straight blades generates intense tangential jet in the tank.

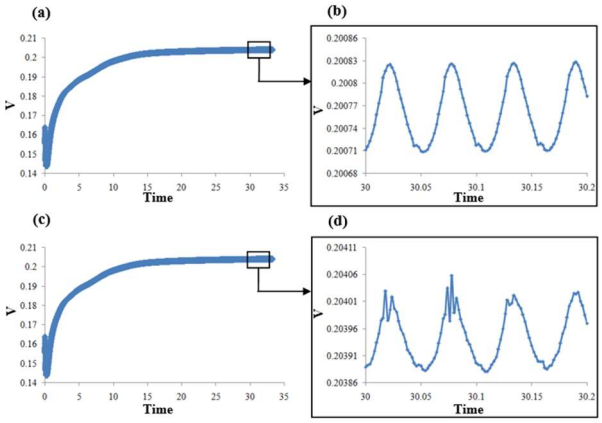

Fig. 5. Time history of the tangential velocity component V

5.1.3 Axial velocity component

Fig. 6(a) depicts the evolution of the axial velocity component over time with the use of a CFD code. In Fig. 6(b), the evolution of the axial velocity is plotted against the time for the strong coupling algorithm that examines the interaction between the turbine impeller and the baffles. Based on these results, we see the appearance of weak periodic fluctuations of the axial velocity component due to the weak interaction between the stirrer and baffles. However, we noted that the tangential component is very low during the passage of the chicane before the blade (point A). This proves that in the area swept by the turbine is the axial component of very low area, it is dominated by the centrifugal force of the turbine. Overall, we see that the problem of interaction does not affect the axial velocity component to the great similarity between the two temporal evolution curves.

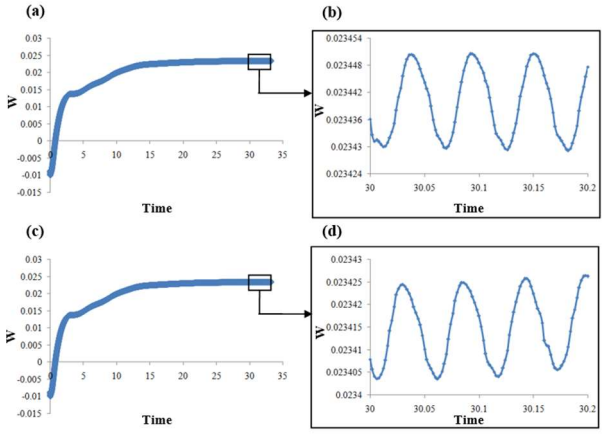

Fig. 6. Time history of the axial velocity component W

5.1.4 Turbulent kinetic energy

Fig.7 shows the history time of the turbulent kinetic energy at the edge of the blade from 32 second. Based on these results, we have noticed that the maximum level of turbulent kinetic energy reaches during the passage of the blade through the point A, but the minimum is achieved between two successive baffles. From these results, we see the disruption during the passage of the baffle before the blade (point A) due to the deformation of the blade. We note that the disruption is low due to the weak interaction between the turbines and baffles.

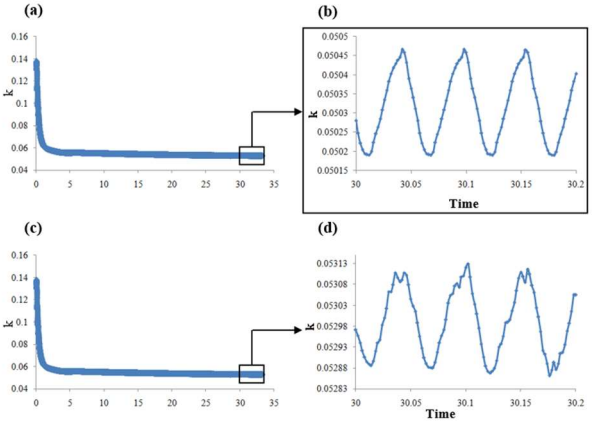

Fig. 7. Time history of the turbulent kinetic energy

5.1.6 The dissipation rate of the turbulent kinetic energy

The history time of the dissipation rate of the turbulent kinetic energy is shown in Fig. 8. From these results, we have noted that the peak value of dissipation rate is reached while going from the baffle through point A. However, the minimum value is reached between two successive baffles. Overall, the rate of dissipation of the turbulent kinetic energy shows periodic fluctuations during the passage of the baffle before the blade, which is seen in Fig. 8(a) and (b) with and without the coupling algorithm, respectively.

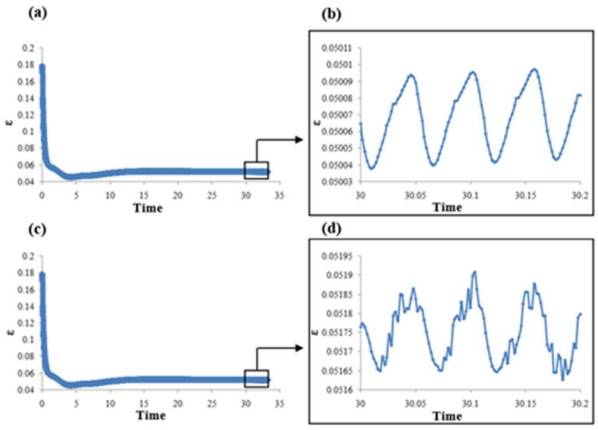

Fig. 8. Time history of the dissipation rate of the turbulent kinetic energy

However, in the Fig. 8(b), the disruptions when the chicane passed by the point (A). This proves that these disturbances happen, mainly, due to the displacement of the blade because of the problems of interaction between the turbine and the fluid. Therefore, we can conclude that the interaction problems directly affect changes in the dissipation of turbulent kinetic energy levels.

5.2 At Baffles (point B)

5.2.1 The three components of velocity

Fig. 9, Fig. 10 and Fig. 11 show the evolution over time of the three components of the velocity at point (B) located at the baffles. The temporal evolution of these three components of velocity is presented in a regime from 15000 time steps that correspond to 30 seconds. Overall, there are very significant periodic fluctuations because of the proximity of point (B) for measuring the baffles.

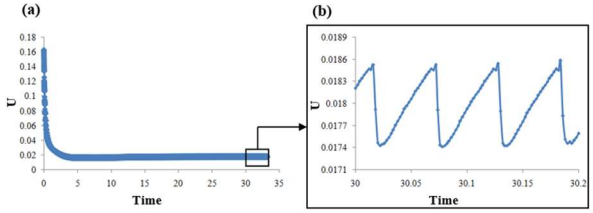

Fig. 9. Time history of the radial velocity component U

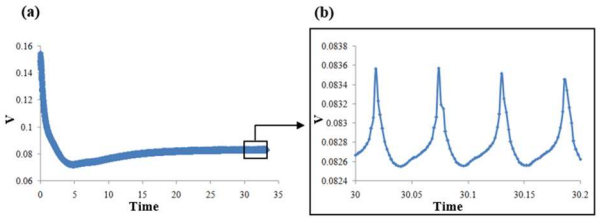

Fig. 10. Time history of the tangential velocity component V

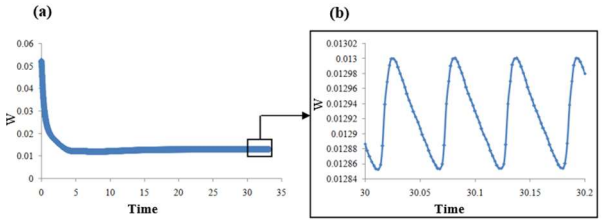

Fig. 11. Time history of the axial velocity component W

The temporal evolution of these three components of velocity is performed for 0.2 second, which corresponds to 100 time steps (time step = 0.002).

The period of fluctuation is constant. Beyond the area swept by the turbine, the fluctuations of the three velocity components are much smaller than those at the blade. Both tangential and axial velocity components are highest during the passage of the baffle in front of the blade of the turbine and they decrease progressively beyond the delivery zone. However, the radial component of the velocity increases between the two baffles successively, since the axial jet transforms into a radial jet at the proximity of the sidewall.

5.2.2 The turbulent kinetic energy

Fig.12 and Fig. 13 show the evolution over time of the turbulent kinetic energy and its dissipation rate at point (B) located at the baffles. The history time of the turbulent kinetic energy and its dissipation rate is presented in a regime from 15000 time steps that corresponds to 30 seconds. Fig.12.b and Fig. 13.b present an expansion of 100 time steps of a portion of the temporal evolution from 15000 time steps (Fig.12.a, and Fig. 13.a).

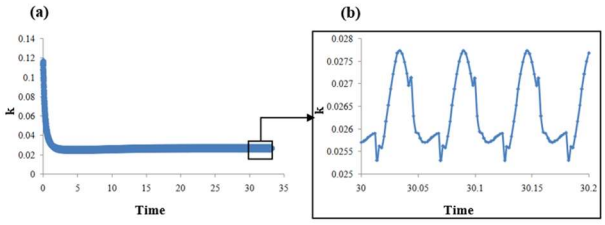

Fig. 12. Time history of the turbulent kinetic energy

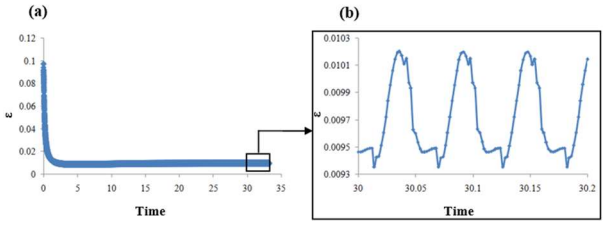

Fig. 13. Time history of the dissipation rate of the turbulent kinetic energy

Near the baffle, the fluctuations of the turbulent kinetic energy and its dissipation rate are constant periodic intervals. There was, also, a decrease of fluctuations in turbulent kinetic energy and its dissipation rate over time compared to those presented at the end of the blade. Moreover, we can deduce that the use of a coupling algorithm does not have a great interest in view the absence disruptions due to deformation of the blade since the point (B) visualization is far from the blades.

5.3. Downstream of the blade (point C)

5.3.1 History time of pressures

The history time of the pressure on the downstream of the blade (point C) is shown in Fig. 14. From these results, we notice the presence of weak periodic fluctuations that are spread over 0.2 second because of the weak interaction between the baffle and the turbine. At each period, we observe a passage between a maximum and a minimum value corresponding to the passage of the front baffle (point C). The highest values have pressure points downstream of the baffle. However, low values demonstrate the presence of the depression zones upstream of the baffle. Otherwise, values situated between two highest peaks correspond to the passage of the median plane between two successive baffles in front of the chosen point.

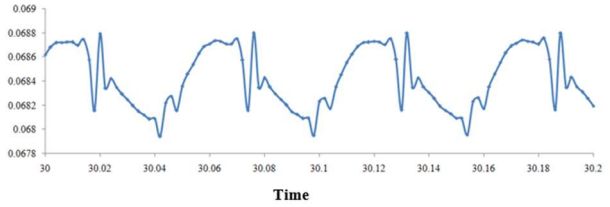

Fig. 14. Time history of pressures

5.3.2 History time of displacement of the blade

Fig. 15 shows the history time of the blade displacement in a given point at the end of the blade (C). From these results, we see that the shape of the curve of the temporal evolution of this movement very low periodic fluctuation. In each period, the displacement has rapidly changed between a maximum peak and minimum time. This indicates the portion of the baffle in front of the point C. Moreover, we note that fluctuations in the movement of the blade coincide with the periodic pressure oscillations presented in 0.2 seconds. This means that the variation of the pressure directly affects the deformation of the blade.

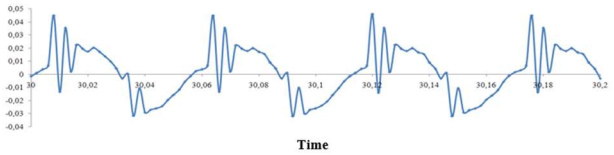

Fig. 15. Time history of displacement

5.3.3 Comparative study between the stationary approach and unsteady approach

Fig. 16 shows the history time of the blade displacement fields. Under these conditions, it was assumed that the deformations of the axis of the turbine caused by the distortion are negligible minor/slight deformation of the blades.

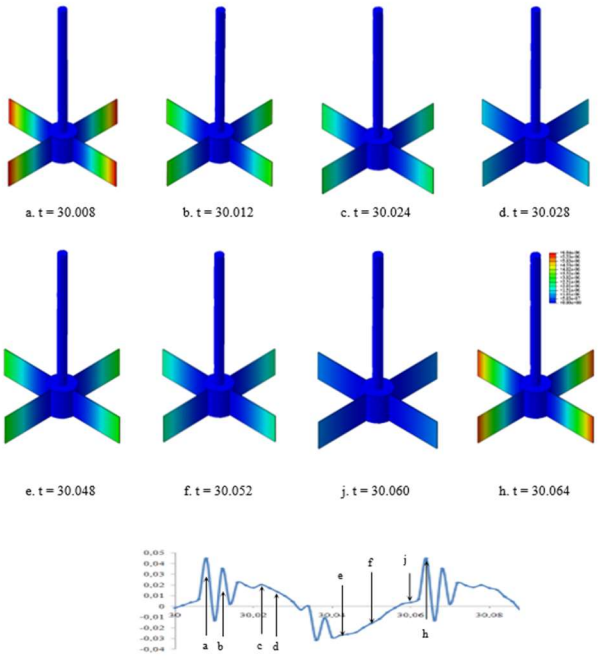

Fig. 16. Evolution of the displacement field of the blade

This figure, also, shows that the maximum values are present at the instants t = 30.008 and t = 30.064

seconds. Corresponding to 15,000 time steps (Fig. 16.a), respectively.

5.3.4 Comparison with anterior results

Fig. 17 shows the axial development of the radial component of the velocity U (z) in both steady and unsteady approaches. These profiles are presented for three dimension radial positions equal to r = 0.5, r = 0.566, r = 0.66, r = 0.7 and r = 0.766, respectively. From these results, we notice that different gaits present parabolic branches and the maximum value is reached at an axial position equal to z = 1. In this respect, the highest values are already obtained in a radial position r = 0.5. Actually, the result is already expected because the area where the discharge of the fluid is very important and it is at the end of the blade. The comparison between the results obtained using steady and unsteady two approaches leads us to the fact that the use of both approaches can be used every two. Despite that, the unsteady approach is more reliable and more complete, steady approach can predict the hydrodynamic characteristics of the flow without providing the effect of the interaction between the fluid and the turbine.

Furthermore, we compared the performance of our approach to the experimental values of [34]. Based on these results, there is a great agreement between the two results and this proves the validity of the adopted method of analysis.

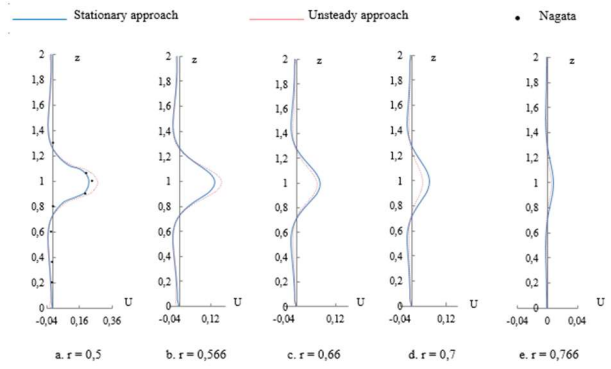

Fig. 17. Axial profiles of the dimensionless radial velocity component

6. Conclusion

In this paper, a strong coupling algorithm is used between two codes of Computational Fluid Dynamics (CFD) and Computational Structure Dynamics (CSD) for numerical simulation of interaction problems in a stirred vessel equipped with a four turbine blades. This work allowed us to follow the evolution of the unsteady fluid. In fact, the results are presented for 0.2 seconds, which corresponds to 100 time steps (1 step = 0.002 second time) when the plan is established from 30 seconds. More specifically, we have shown the history time of the hydro-mechanic parameters, namely, the compounds of velocity, the characteristics of the turbulence, the pressure and deformation of the turbine, all at three points in the delivery zone of the turbine and at the chicane. These results showed that the evolution is constant when the plan is established from 30 s. Actually, when an enlargement of the curve - obtained by a CFD code - is made, some periodic fluctuations are observed. However, the use of the strong coupling algorithm results in the appearance of other disturbances, hence the interaction between the turbine blade and the fluid.

7. Nomenclature

d	turbine diameter, m
D	internal diameter of the vessel tank, m
Fr	Froude number, dimensionless, $Fr = \frac{(2\ \pi N)^2 d}{g}$
G	turbulent kinetic energy production, dimensionless
g	gravity acceleration, $m^2 .s^{-1}$
h	turbine position, m
H	vessel tank height, m
k	turbulent kinetic energy, dimensionless
N	velocity of turbine impeller, rad. s^{-1}
N_P	power number, dimensionless, $N_P = \frac{P}{\rho N^3 d^5}$
P	power, W

p	pressure, dimensionless
Re	Reynolds number, dimensionless
r	radial coordinate, dimensionless
s	shaft diameter, m
S_Φ	sink term, dimensionless
t	time, s
U	radial velocity components, dimensionless
V	angular velocity components, dimensionless
W	axial velocity components, dimensionless
z	axial coordinate, dimensionless
$\vec{u}$	displacement vector
$\vec{V}$	velocity vector of the fluid
$\overrightarrow{V_s}$	velocity vector of the structure
$\vec{J}_\Phi$	flux term vector
$\bar{\bar{I}}$	identity tensor
$\vec{f}$	force vector
$\vec{n}$	normal vector

Greek symbols

μ	viscosity, Pa.s
ρ	density, kg.m^3
ε	dissipation rate of the turbulent kinetic energy, dimensionless
θ	angular coordinate, rad
υ_t	turbulent viscosity, dimensionless
σ_k	constant in the standard k-ε model
Γ_Φ	diffusion coefficient, dimensionless
Φ	general transport parameter, dimensionless
$\bar{\bar{\sigma}}$	stress tensor of the structure
$\bar{\bar{\varepsilon}}$	strain tensor of the structure
$\bar{\bar{\tau}}$	stress tensor of the fluid

Abbreviations

CFD	Computational Fluid Dynamics
CSD	Computational Structure Dynamics
CSS	Conventional Serial Staggered
FSI	Fluid-Structure Interaction
f	fluid
s	structure

8. References

[1] J. Mackerle, Fluid-structure interaction problems, finite elements and boundary elements approaches. A bibliography (1995–1998). Finite Elements Analysis Design 31 (1999) 231–240.

[2] F. Casadei, J.P. Halleux, A. Sala, F. Chille, Transient fluid-structure interaction algorithms for large industrial applications. Computer Methods in Applied Mechanics and Engineering 190 (2001) 3081–3110.

[3] N. Bodard, M.O. Deville, Fluid–structure interaction by the spectral element method. Journal of Scientific Computing 27 (2006) 123–136.

[4] Y. Wang, Combination of CFD and CSD packages for fluid-structure interaction. Journal of Hydrodynamics 20 (2008) 756–761.

[5] K. Billah, R. Scanlan, Tacoma Narrows Bridge Failure, and Undergraduate Physics Textbooks. American Journal of Physics 59 (1991) 118–124.

[6] C. Farhat, K.G. van der Zee, P. Geuzaine, Provably second-order time-accurate loosely-coupled solution algorithms for transient nonlinear computational aeroelasticity. Computer Methods in Applied Mechanics and Engineering 195 (2006) 1973–2001.

[7] K. Willcox, J. Paduano, J. Peraire, Low order aerodynamic models for aeroelasticcontrol of turbomachines, in: 40th AIAA/ASME/ASCE/AHS/ASC Structures. Structural Dynamics and Materials Conference, St Louis, MO, USA, (1999) 1–11.

[8] J.F. Gerbeau, M. Vidrascu, P. Frey, Fluid-structure interaction in blood flows on geometries based on medical imaging. Computers & Structures 83 (2005) 155–165.

[9] W. Wall, T. Rabczuk, Fluid-structure interaction in lower airways of CT-basedlung geometries. International Journal for Numerical Methods in Fluids 57 (2008) 653–675.

[10] C. Peskin, Numerical analysis of blood flow in the heart. Journal of Computational Physics 25 (1977) 220–252.

[11] C. Peskin, Flow patterns around heart valves: a numerical method. Journal of Computational Physics 10 (1972) 252–271.

[12] K. Dumont, J. Vierendeels, R. Kaminsky, G. Van Nooten, P. Verdonck, D. Bluestein, Comparison of the hemodynamic and thrombogenic performance of two bileaflet mechanical heart valves using a CFD/FSI model. Journal of Biomechanical Engineering – Transactions of the ASME 129 (2007) 558–565.

[13] P. Crosetto, Reymond, S. Deparis, D. Kontaxakis, N. Stergiopulos, A. Quarteroni, Fluid-structure interaction simulation of aortic blood flow. Comput Fluids 43 (2011) 46–57.

[14] C.J. Greenshields, H.G. Weller, A unified formulation for continuum mechanics applied to fluid–structure interaction in flexible tubes. International Journal for Numerical Methods in Engineering 64 (2005) 1575–1593.

[15] E. Walhorn, A. Kolke, B. Hubner, D. Dinkler, Fluid–structure coupling within a monolithic model involving free surface flows. Comput Struct 83 (2005) 2100–2111.

[16] M. Heil, A.L. Hazel, J. Boyle, Solvers for large–displacement fluid–structure interaction problems: segregated versus monolithic approaches. Computational Mechanics, 43 (2008) 91–101.

[17] S. Badia, Q. Quaini, A. Quarteroni, Modular vs. non-modular preconditioners for fluid–structure systems with large added-mass effect. Computer Methods in Applied Mechanics and Engineering 197 (2008) 4216–4232.

[18] F. Cirak, R. Deiterding, S.P. Mauch, Large-scale fluid–structure interaction simulation of viscoplastic and fracturing thin-shells subjected to shocks and detonations. Comput Struct 85 (2007) 1049–1065.

[19] A. Karac, B. Blackman, V. Cooper, A. Kinloch, S.R. Sanchez, W. Teo, Modelling the fracture behaviour of adhesively-bonded joints as a function of test rate. Engineering Fracture Mechanics 78(6) (2011) 973–989.

[20] C. Kassiotis, A. Ibrahimbegovic, R. Niekamp, H. Matthies, Nonlinear fluid structure interaction problem. Part I: implicit partitioned algorithm, nonlinear stability proof and validation examples. Comput Mech 47 (2011) 305–323.

[21] C. Habchi, S. Russeil, D. Bougeard, J.L. Harion, T. Lemenand, A. Ghanem, D. Della Valle, H. Peerhossaini, Partitioned solver for strongly coupled fluid–structure interaction. Computers & Fluids 71 (2013) 306–319.

[22] M.A. Fernández, M. Moubachir, A Newton method using exact Jacobians for solving fluid–structure coupling, Comput. Struct. 83(2–3) (2005) 127–142.

[23] J. Degroote, P. Bruggeman, R. Haelterman, J. Vierendeels, Stability of a coupling technique for partitioned solvers in FSI applications, Comput. Struct. 86(23–24) (2008) 2224–2234.

[24] S. Badia, F. Nobile, C. Vergara, Robin–Robin preconditioned Krylov methods for fluid–structure interaction problems. Computer Methods in Applied Mechanics and Engineering 198 (33–36) (2009) 2768–2784.

[25] H. Baek, G.E. Karniadakis, A convergence study of a new partitioned fluid–structure interaction algorithm based on fictitious mass and damping. Journal of Computational Physics 231 (2012) 629–652.

[26] G. Sieber, Numerical Simulation of Fluid-Structure Interaction Using Loose Coupling Methods. PhD thesis, at the Department of Numerical Methods in Mechanical Engineering, Darmstadt University of Technology (2002).

[27] M. Glück, M. Breuer, F. Durst, A. Hlfmann, E. Rank, Computation of wind-induced vibrations of flexible shells and membranous structures. Journal of Fluids and Structures 17 (2003) 739–765.

[28] E. Bucchignani, F. Stella, F. Paglia, 2004. A partition method for the solution of a coupled liquid-structure interaction problem. Applied Numerical Mathematics 51, 463–475.

[29] M.S. Abid, C. Xuereb, J. Bertrand, Hydrodynamics in vessels stirred with anchors and gate agitators: Necessity of a 3-D modeling. T. Instn. Chem. Eng. 70 (1992) 377–384.

[30] S.M.C.P. Pedrosa, J.R. Nunhez, The behavior of stirred vessels with anchor type impellers. Computers & Chemical Engineering 24 (2000) 1745–1751.

[31] F. Savreux, P. Jay, A. Magnin, Viscoplastic fluid mixing in a rotating tank. Chemical Engineering Science 62 (2007) 2290–2301.

[32] M. Baccar, M.S Abid, Caractérisation de l'écoulement turbulent et du transfert thermique générés par des mobiles ancre et barrière dans une cuve agitée. International Journal of Thermal Sciences 38 (1999) 892–903.

[33] B. Triveni, B. Vishwanadham, S. Venkateshwar, Studies on heat transfer to Newtonian and non-Newtonian fluids in agitated vessel. Heat Mass Transfer 44 (2008) 1281–1288.

[34] S. Nagata. Mixing: principles and applications. John Wiley & Sons: Halstead press,Japan, (1975).

[35] S.V. Patankar. Numerical heat transfers and fluid flow. Series in Computational Methods in Mechanics and Thermal Sciences, Mc Graw Hill, New York, (1980).